Adaptive flight control system for flight safety improvement in reentry and other high-velocity vehicles

A.V. Efremov [*,#], E.V. Efremov [#], M.S. Tiaglik [#], I. Kh Irgaleev [#], A.I. Shcherbakov [#], Z. Mbikayi [1]

ABSTRACT

An adaptive controller and a nonlinear rate limiter are presented in order to improve the flight safety of manually controlled reentry vehicles and supersonic transport (SST) aircraft. The adaptive controller is based on the principle of dynamic inversion. The calculation of the controller parameters corresponding to the aerodynamic coefficients of the vehicle was carried out by a proposed online identification procedure. The effectiveness of the adaptive controller was tested through a set of experiments performed using a ground-based simulator. The obtained results were used to estimate the probability of an accident due to pilot error for the basic Space Shuttle flight control system and for its improved version with the adaptive controller. It was found that using the adaptive controller causes high required rates of elevon deflection. Because of the actuator's rate limiting, this is a source of pilot-induced oscillations. To counteract these oscillations in the pilot-vehicle closed loop system, an adaptive nonlinear rate limiter is introduced. The effectiveness of using the adaptive prefilter for improving the flight safety and flying qualities of the Space Shuttle reentry vehicle and an SST was demonstrated in experiments involving a ground-based simulator.

1. Introduction

Aerospace flight safety is a broad research area, which has specialists from numerous fields involved. Some of the main topics in the field are: protection from space debris and micrometeorites [1,2], safety during launch [3], fire safety onboard spacecraft [4,5], radiation hazards [6], and various aspects of flight control [7,8]. The present paper falls into the last category, as it considers the flight safety problem from a flight control perspective.

The flight control system of modern vehicles can be categorized as a highly augmented system, determining the vehicle dynamics. Failure of such a system leads to a sharp degradation of flying qualities. It considerably deteriorates piloting accuracy and increases the risk of an accident. Because of this, the reliability requirements for flight control are very high. It particular, the international aeronautical community has decided that the probability of a malfunction of the flight control system has to be less than 10^{-9} per hour of flight.

In aviation, a considerable number of piloting tasks are performed manually. Several missions carried out with space vehicles (docking with the ISS, Moon landing, landing of reentry vehicles) were previously performed as manual control tasks as well. Considerable experience in the study of manual control was accumulated in the aeronautical field in the last century, and these methods can be adapted for manual control of spacecraft, reentry vehicles. In addition, an analysis of existing literature demonstrated that a number of aeronautical and reentry vehicles have a number of common flight safety problems when operating at subsonic speeds, especially the issues pertaining to pilot-induced oscillations (PIOs) [9,10]. As can be seen in the Space Shuttle, or the Concorde SST, it is common practice to design reentry vehicles and SSTs with delta wings and use elevons as the control surfaces. Such configurations are characterized by the instantaneous center of rotation being located in front of the pilot's seat. It causes the so-called "reverse control", which is the non-minimum phase behavior of a dynamic system. This peculiarity can be one of the sources of pilot-induced oscillations. Both types of vehicles are characterized by considerable values of the ratios of moments of inertia I_z/I_x and I_y/I_x close to 7–8 [11]. This leads to a strong coupling between longitudinal and lateral motions, as well as yaw and roll motions. The Space Shuttle and the Russian Buran were statically unstable at subsonic speeds. Such unstable configurations are currently

---

* Corresponding author. Corresponding athor:
  E-mail address: pvl@mai.ru (A.V. Efremov).
\# Moscow Aviation Institute.
1 Technical University of Munich.

considered for second-generation supersonic transports.

These and other peculiarities define the unsatisfactory flying qualities character of this type of vehicle. And because of the unambiguous relationship between flying qualities and flight safety indicators [12, 13], it considerably increases the risk of accidents. All this requires significant augmentation of these vehicles by installing feedback loops with high gain coefficients, PI controllers, several filters, etc. In general, such a high level of automation allows to improve flying qualities. However, high values of feedback coefficients cause an increase in the required rates of control surfaces deflection. For reentry vehicles (for example, the Space Shuttle and the Buran), the actuator rate limits $\dot{\delta}_{max}$ are 15–20 *deg*/sec due to unpowered landing. A combination of such low values of $\dot{\delta}_{max}$ and high feedback gains can lead to a very dangerous category of pilot-induced oscillations [14,15] (Category II PIOs, according to the classification given in Ref. [16]). This category is characterized by severe oscillations with amplitudes well into the range where rate and/or position limits become dominant. A rate-limited actuator causes the addition of an amplitude-dependent lag phase shift in the vehicle dynamics and the setting of the amplitude of the limit cycle. To deal with this issue, several versions of nonlinear prefilters were studied for installation in the flight control system of the Russian Buran reentry vehicle [17,18]. Their shortcoming was the additional phase delay, which is an additional source of PIO events. Sufficient phase delay is also characteristic of the Space Shuttle. Its equivalent time delay is close to 0.174 s [19]. The solution proposed for PIO elimination in the Space Shuttle [20] is characterized by considerable variability of the gain coefficient, causing the necessity of pilot adaptation. The input signal of both prefilters was the pilot control signal. Such installation of the limiters effectively did not influence the feedback signals, which also have high rates. Another problem that arises when using these traditional flight control laws for the considered vehicles, is their implementation in a wide range of the velocities and altitudes. There is increased complexity of gain scheduling along the entire flight envelope and the reconfiguration of the control law in case of failures or faults.

For these reasons, new approaches to flight control system design, allowing to implement adaptive and robust features, are more desirable.

Feedback linearization is one of the methods often used in the nonlinear dynamic inversion scheme in order to cancel the system nonlinearities, which then allows to use linear control techniques [21–23]. This method, however, requires extensive knowledge and understanding of the dynamical system under study. This requirement is almost impossible to satisfy because there are always uncertainties present in real systems. A popular approach to solving this problem is by combining nonlinear dynamic inversion with robust control methods such as μ synthesis or H-infinity control [24,25]. Using this approach has been quite effective, but still not all uncertainties are considered, or some known nonlinear dynamics are considered as uncertainties. The resulting control system can therefore be marginally or overly conservative in performance and stability robustness [26]. To solve these issues, incremental nonlinear dynamic inversion was developed, first as simplified nonlinear dynamic inversion [27,28].

This method has been widely applied to various aerospace systems [29–33].

Incremental nonlinear dynamic inversion (INDI) works by feeding back synchronous sensor measurement or estimation of control deflection and angular acceleration. This reduces the requirement of accurate knowledge of the vehicle dynamics to knowledge of the control effectiveness matrix. The INDI method, however, is very sensitive to time delays which are always present in real systems [34]. There have been solutions developed to solve these issues, but those are beyond the scope of this paper.

Another popular method used in control design is classical gain scheduling, which has been studied comprehensively for all kinds of systems and in all kinds of configurations [35–39]. The main idea of the method is based on linear time-varying plants. By having several linear

models obtained at various operating points throughout the operation envelope of the system, it is possible to use linear controllers computed for each operating point. Then the controllers can be scheduled using some predefined scheduling variable.

Besides the feedback linearization and gain scheduling-based methods, there have been other methods developed that are Lyapunov-based. One of them is sliding mode control [40–42]. As the name suggest, the sliding mode control technique tries to make the system slide along a cross section of its normal behavior by applying certain classes of discontinuous control signals. However, in essence, applying discontinuous signals means the structure of the controller changes. This brings the method close to gain scheduling.

The classes of methods discussed above can be considered as deterministic algorithms. Current advances in data science and machine learning gave rise to a generation of new methods that are nondeterministic in nature, in control theory in general and flight control in particular.

This paper proposes the use of an approach to the control law design problem based on the principle of dynamic inversion and adaptive control. The proposed controller consists of a baseline controller synthesized using dynamic inversion and adaptive augmentation based on a modification of the least squares algorithm. The modifications made allow the algorithm to perform system identification much faster than the usual recursive least squares method. This approach allows to optimize the flying qualities in the entire flight envelope, while minimizing the implementation effort, and to provide the necessary robustness. Additionally, there is a nonlinear prefilter, which is a modification of the SAAB rate limiter [43]. The proposed limiter allows to stay within the actuator rate limits without a significant increase in the effective phase delay and provides a considerable decrease in the variance of error in comparison with its prototype.

The potentials of both means for improving flying qualities and flight safety in reentry vehicles and SSTs are tested using a ground based simulator.

2. Control law design

The control law design procedure presented in this paper can be divided into two stages. The first stage is the design of a baseline controller based on the nonlinear dynamic inversion principle, and the second stage is adaptive augmentation based on a least square approach.

2.1. Baseline nonlinear dynamic inversion (NDI) control law

The baseline control law is represented as nonlinear dynamic inversion (NDI) architecture, based on feedback linearization as given in Ref. [44], through which the aircraft dynamics are canceled using prior knowledge of said dynamics.

Let the aircraft be described by a set of differential equations as

$$\dot{x}(t) = f(x) + \gamma(x)u \tag{1}$$

$$y = d(x) \tag{2}$$

where $x \in R^n$ is the state vector, $u \in R^m$ is the input vector, and $y \in R^m$ is the output vector.

We can differentiate the output expression in Equation (2) with respect to x and get the following expression:

$$\dot{y} = \frac{\partial d}{\partial x}\dot{x} = \frac{\partial d}{\partial x}f(x) + \frac{\partial d}{\partial x}\gamma(x)u = F(x) + \Gamma(x)u \tag{3}$$

If the goal is to make the output, $\dot{y}$, equal to some pseudo-input, ν, then the input u that achieves this can be found by inverting Equation (3):

$$u = \Gamma^{-1}(x)[\nu - F(x)] \tag{4}$$

A.V. Efremov et al.
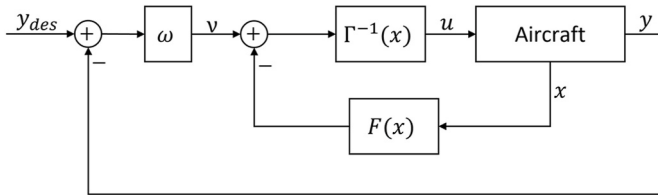
Fig. 1. Schematic of nonlinear dynamic inversion control.

The desired pseudo-input, ν, can be computed by an error controller, such that

$$\nu = (y_{des} - y)\omega \tag{5}$$

where y_{des} is the desired output, y is the measured output, and ω is the desired bandwidth of the closed-loop system.

It is worth noting that an integrator can also be added to the error controller in order to improve the robustness of the closed-loop system or fix the steady-state error.

A schematic representation of this control law ("the baseline controller") can be seen in Fig. 1.

From Equation (3), it is easy to see that if the partial derivatives are evaluated at some given operating point (u_0, x_0), then $F(x)$ and $\Gamma(x)$ will respectively correspond to matrices A and B of the nonlinear system linearized at (u_0, x_0). If the system can be linearized online, then matrices A and B can be used directly in the scheme shown in Fig. 1. This is, in fact, the basis of adaptive augmentation, presented in the next subsection.

2.2. Adaptive augmentation

Adaptive augmentation follows an indirect adaptive control scheme in which an identification algorithm is run to identify matrices A and B, which are then used in the control scheme shown in the previous subsection.

A mean square minimization algorithm is used for system identification. The algorithm makes use of a replay buffer that stores a fixed amount of latest flight data points. This means there is a moving window of data used for linear system identification.

Proceeding from the assumption made in Ref. [45] that a nonlinear system can be approximated by piecewise linear systems, the linear systems identified using the moving window of data can be understood as local linear approximations of the nonlinear system at each time step or at the intervals used between each identification.

This process goes as follows:

Near any operating point, which is the trim value of the aircraft, the linear approximation of a nonlinear system can be written as

$$\dot{x} = A\delta x + B\delta u \tag{6}$$

where $\delta x = x - x_0$, $\delta u = u - u_0$, $A \in R^{n \times n}$ is the state matrix, and $B \in R^{n \times m}$ is the input matrix.

Equation (6) can be rewritten as

$$\dot{x} = Ax + Bu - Ax_0 - Bu_0 \tag{7}$$

The notation in Equation (7) is useful because if the trim values (u_0, x_0) are not considered, then the resulting matrices A and B will not correctly represent the dynamics of the vehicle.

Assuming we can measure a set of l data points, we can get a system of equation (8), which can be rewritten as in Equation (9). Instead of measuring the trim values (u_0, x_0) and adding them in Equation (8), their influence on aircraft motion can be estimated.

$$\begin{cases} \dot{x}_1 = Ax_1 + Bu_1 - Ax_{0_1} - Bu_{0_1} \\ \dot{x}_2 = Ax_2 + Bu_2 - Ax_{0_2} - Bu_{0_2} \\ \vdots \\ \dot{x}_l = Ax_l + Bu_l - Ax_{0_l} - Bu_{0_l} \end{cases} \tag{8}$$
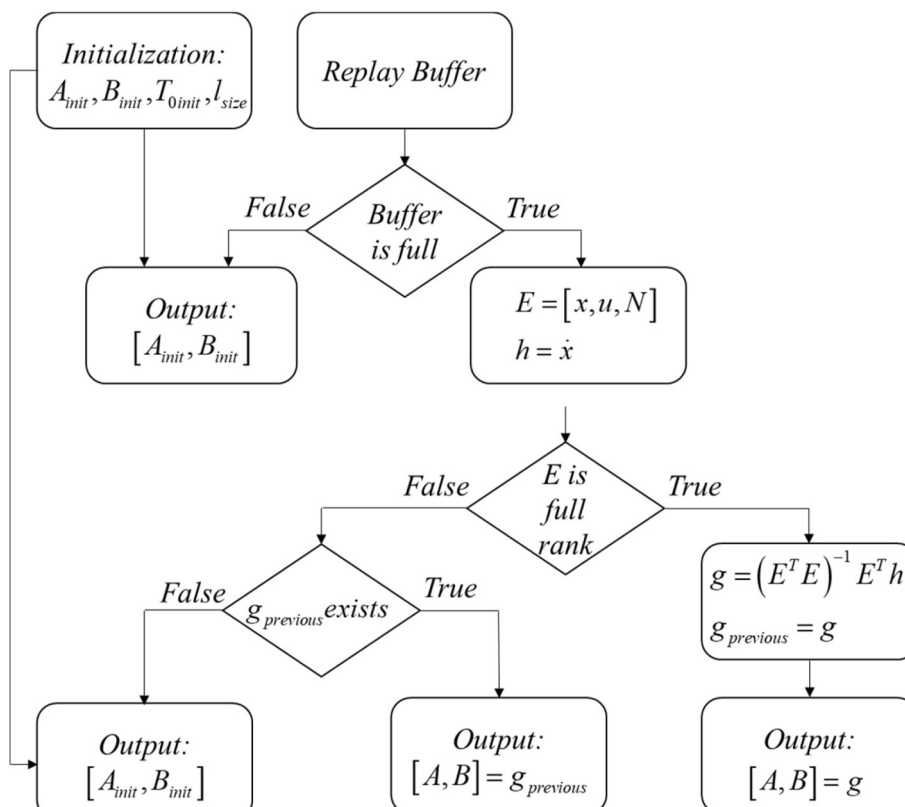

**Fig. 2.** Online identification algorithm.
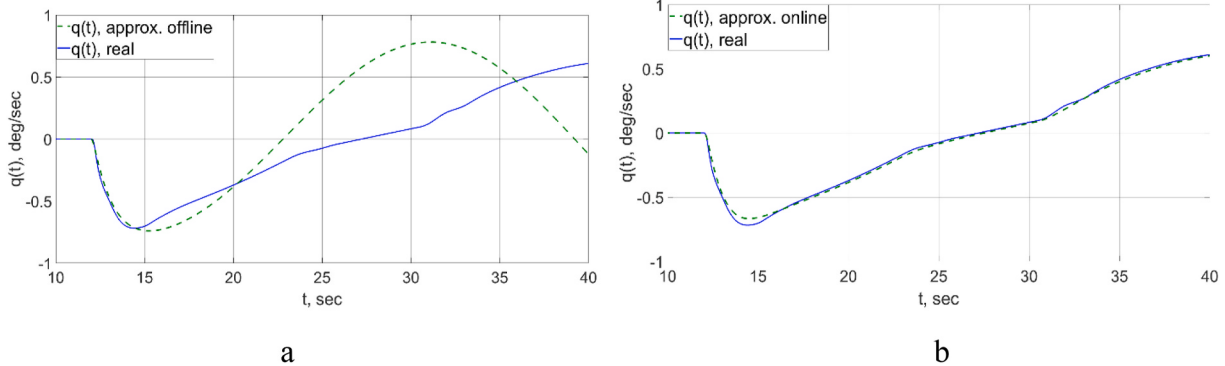
Fig. 3. Comparison of the time responses $q(t)$ obtained by only initial offline identification (a) and online identification (b) with the response $q(t)$ obtained with the real nonlinear model.
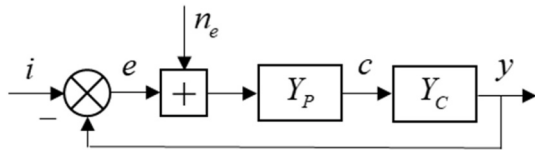

Fig. 4. Compensatory pilot-vehicle system.

**Fig. 5.** MAI's ground-based workstation.
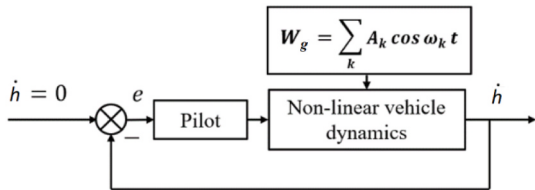
Fig. 6. Pilot-aircraft system in an acceleration task.

Equation (8) can be rewritten as:

$$Eg = h \tag{9}$$

where $E \in R^{l \times (m+n+1)}$ is a matrix of rank $(m + n + 1)$, with $l \geq (m + n + 1)$. Matrix E is created by concatenating vectors $x, u,$ and $N = [1, ... 1]^T \in R^{l \times 1}$, such that $E = [x, u, N]$. g is a matrix containing solutions A, B, and T_0, such that $g = [A, B, T_0]$ where T_0 is a matrix representing moments
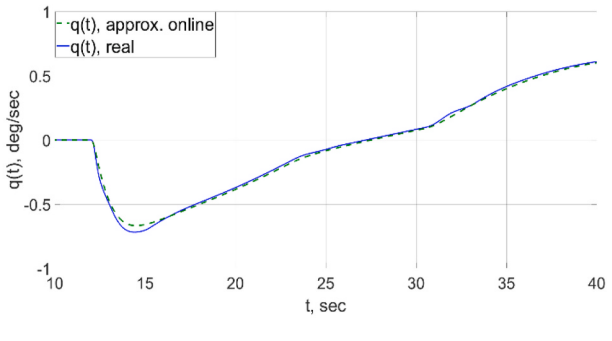
Fig. 7. MAI's ground-based simulator.

determined by the trim values. Then, T_0 can be discarded, and the estimated A and B would perfectly describe the dynamics of the vehicle.

Equation (9) can then be solved as shown in Equation (10), and an online identification algorithm making use of the replay buffer can be designed as shown in Fig. 2.

$$g = \left(E^T E\right)^{-1} E^T h \tag{10}$$

The algorithm shown in Fig. 2 starts by collecting data until the replay buffer is full. During this time, the algorithm outputs the initial guesses of A and B. After the buffer has been filled, matrix E is formed, and checked for fullness of rank. This condition is necessary, because if E is not full rank, then there are infinitely many solutions to the least squares problem as shown below:

For all solutions of g, we have

$$\|Eg - h\|_2 \geq \left\|E\left(\left(E^T E\right)^{-1} E^T h\right) - h\right\|_2 \tag{11}$$

where $\|\cdot\|_2$ is the Euclidean norm. This inequality holds only if

$$g = \left(E^T E\right)^{-1} E^T h + \left(I - \left(E^T E\right)^{-1} E^T E\right)\omega \tag{12}$$

for any vector ω. This provides an infinite number of solutions, unless E is full rank, which means $(I - (E^T E)^{-1} E^T E)$ is a zero matrix. Additionally, if E is not full rank, then there are linearly dependent data points, which means the previously identified model is still valid.

After obtaining matrices A and B, they can then be used in the control scheme shown in Fig. 1.

Assuming the longitudinal dynamics of the aircraft, the differential equations can be written in state-space form as shown in Equation (13).

A.V. Efremov et al.
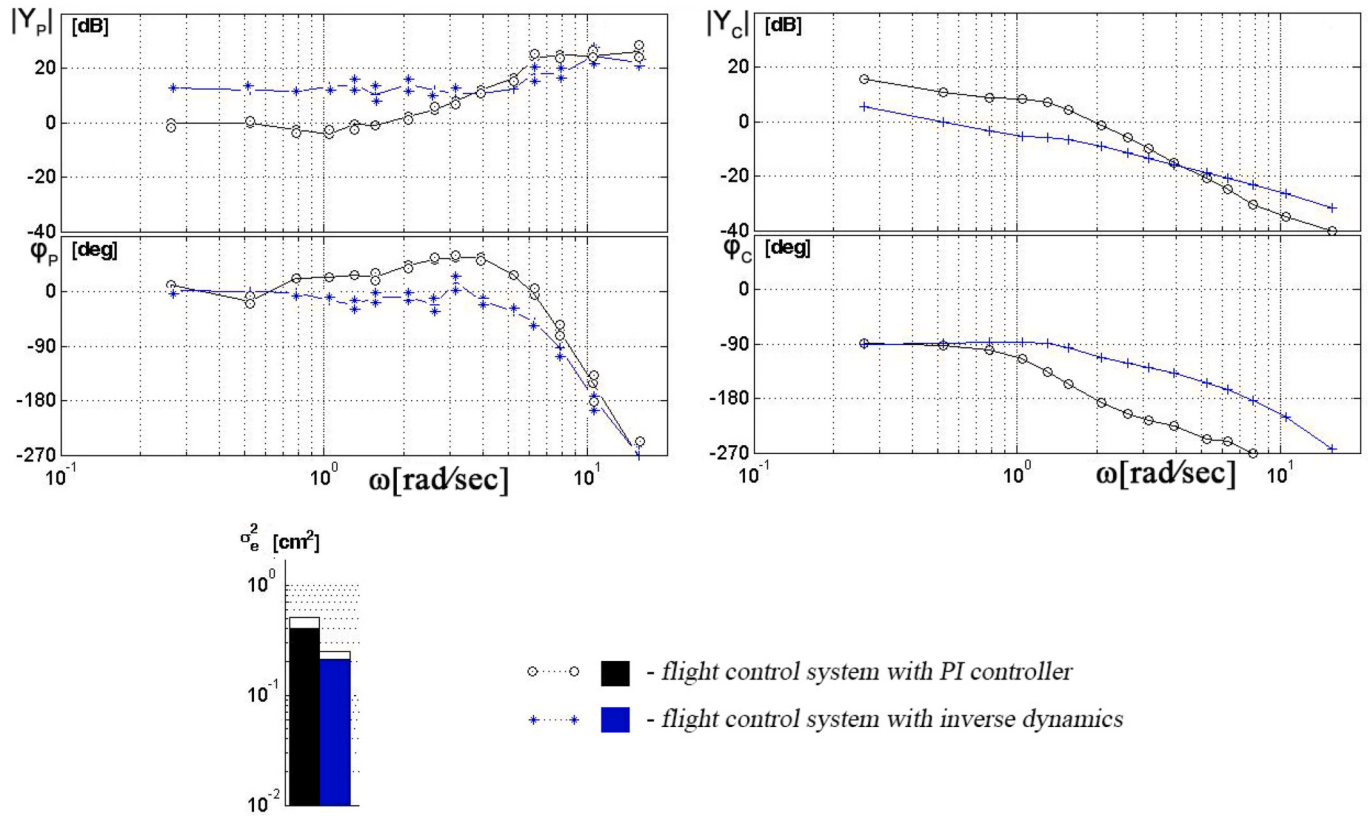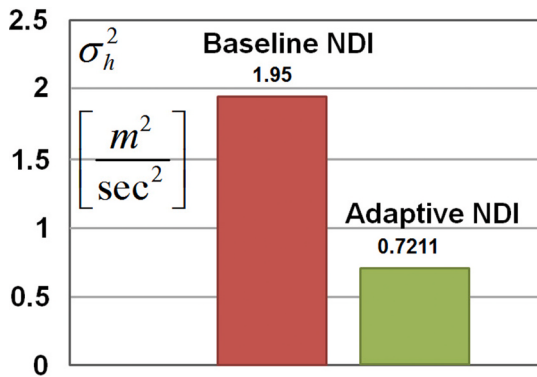
Fig. 8. Experiments on the Space Shuttle dynamics.

Table 1
Pilot ratings.

| Criterion	PR_b	PR_{ad}
$\omega_{BW\theta}, \tau_{e\theta}$	>6.5	~ 3.5
(19)	6.5	4.6

Fig. 9. Variances of $\dot{h}$ for different controllers in an acceleration task.

$$\begin{bmatrix} \dot{u} \\ \dot{w} \\ \dot{q} \\ \dot{\theta} \end{bmatrix} = \begin{bmatrix} X_u & X_w & X_q & X_\theta \\ Z_u & Z_w & Z_q & Z_\theta \\ m_u & m_w & m_q & m_\theta \\ 0 & 0 & 1 & 0 \end{bmatrix} \begin{bmatrix} u \\ w \\ q \\ \theta \end{bmatrix} + \begin{bmatrix} X_\eta \\ Z_\eta \\ m_\eta \\ 0 \end{bmatrix} [\eta] \tag{13}$$

The equation of rotational pitch motion can be rewritten as

$$\dot{q} = m_u u + m_w w + m_q q + m_\theta \theta + m_\eta \eta \tag{14}$$

Doing the same inversion as in Equation (4), we can get the elevator input η that achieves the desired pseudo-input $v = \dot{q}_d$;

$$\eta = \frac{1}{m_\eta} \left[\dot{q}_d - \left(m_u u + m_w w + m_q q + m_\theta \theta \right) \right] \tag{15}$$

The coefficients used in the control law shown in Equation (13) are taken from the A and B matrices computed online.

## 3. Results of adaptive controller assessment and their discussion

3.1. Assessment of the on-line identification procedure

The assessment is done for a nonlinear model of one of the SST configurations. It was developed recently in the process of research carried out within the Program for the Development of the World-Class Research Center "Supersonic" in 2020–2025. As an example, matrixes A and B for this model, calculated for a velocity of 267 km/h, are given below:

$$A = \begin{bmatrix} -0.128 & -0.100 & -0.027 & -0.225 \\ -0.259 & -0.536 & 0.920 & -0.047 \\ 0.157 & 0.578 & -0.845 & 0.070 \\ 0 & 0 & 1 & 0 \end{bmatrix}; B = \begin{bmatrix} -0.068 \\ -0.091 \\ -0.750 \\ 0 \end{bmatrix} \tag{16}$$

The assessment considered below concerns the identification algorithm used for adaptive augmentation. One second of flight data is collected at a frequency of 100 Hz in order to compute an initial approximation of the model. Then, a simulation with a random input signal was run both on the real model and using the identified model, without using the online identification capabilities. The results of this process are shown in Fig. 3a.

As can be seen, after about 4 s, the identified model is no longer valid and starts diverging from the true dynamics. This shows that the approximated linear model corresponds to the nonlinear model at a short interval of time. Then, the online identification algorithm was

A.V. Efremov et al.
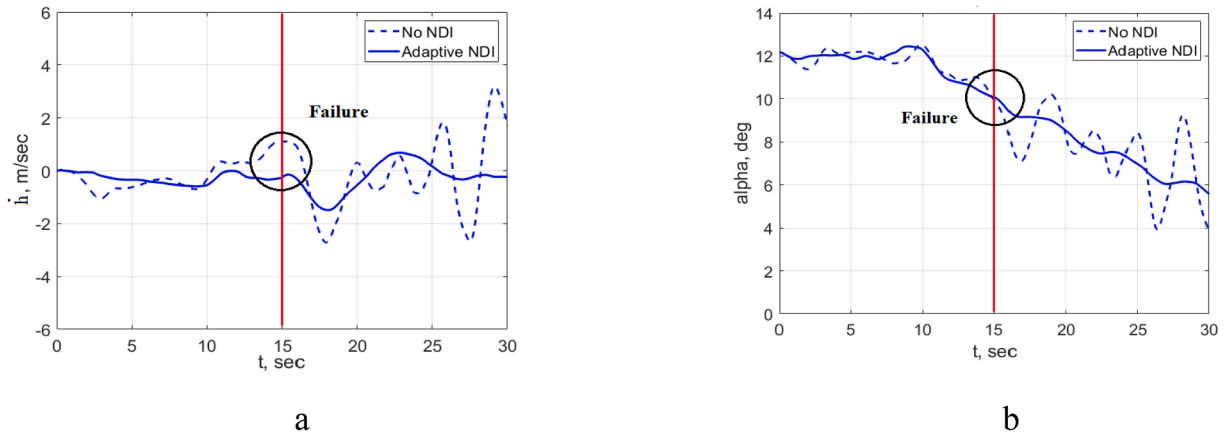
Fig. 10. Time processes of $\dot{h}(t)$ (a) and $\alpha(t)$ (b) in an acceleration task.
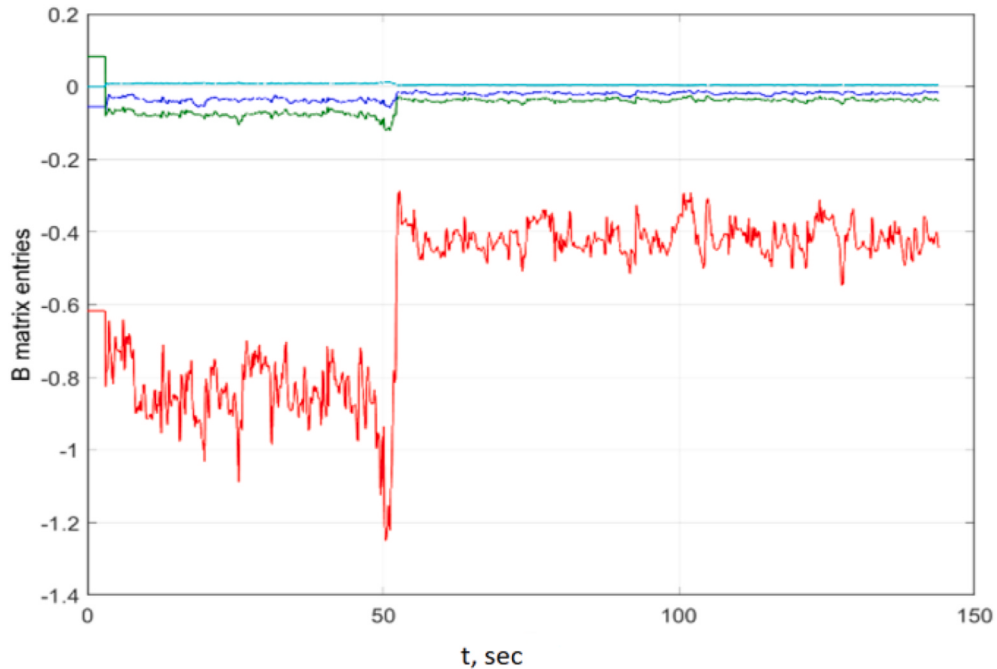
Fig. 11. Adaptation of the coefficients of matrix B.
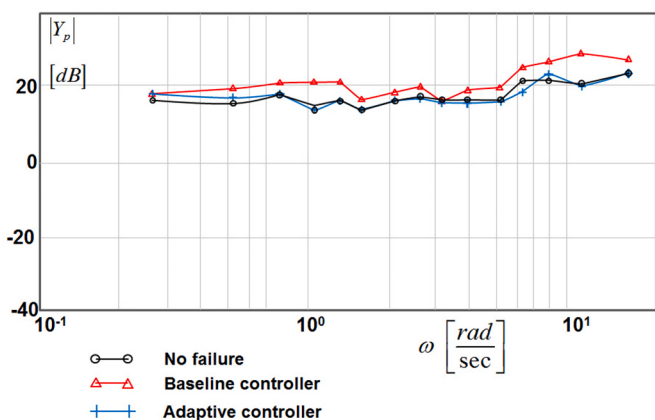
Fig. 12. Pilot frequency response.

activated with the same input signal and the same initial approximation. A comparison between the response $q(t)$ of the real nonlinear model of the SST and its approximated model to a step elevator deflection is shown in Fig. 3b.

3.2. Control law assessment

To assess the control law, several experiments were conducted. These experiments were designed so as to study the behavior of the human pilot, understand the adaptive behavior of the control law in the presence of failures, and estimate the performance of the control law in comparison with traditional strategies.

3.2.1. Experimental design

Two sets of experiments were performed for adaptive controller assessment:

1) experiments on the assessment of a baseline controller;

A.V. Efremov et al.
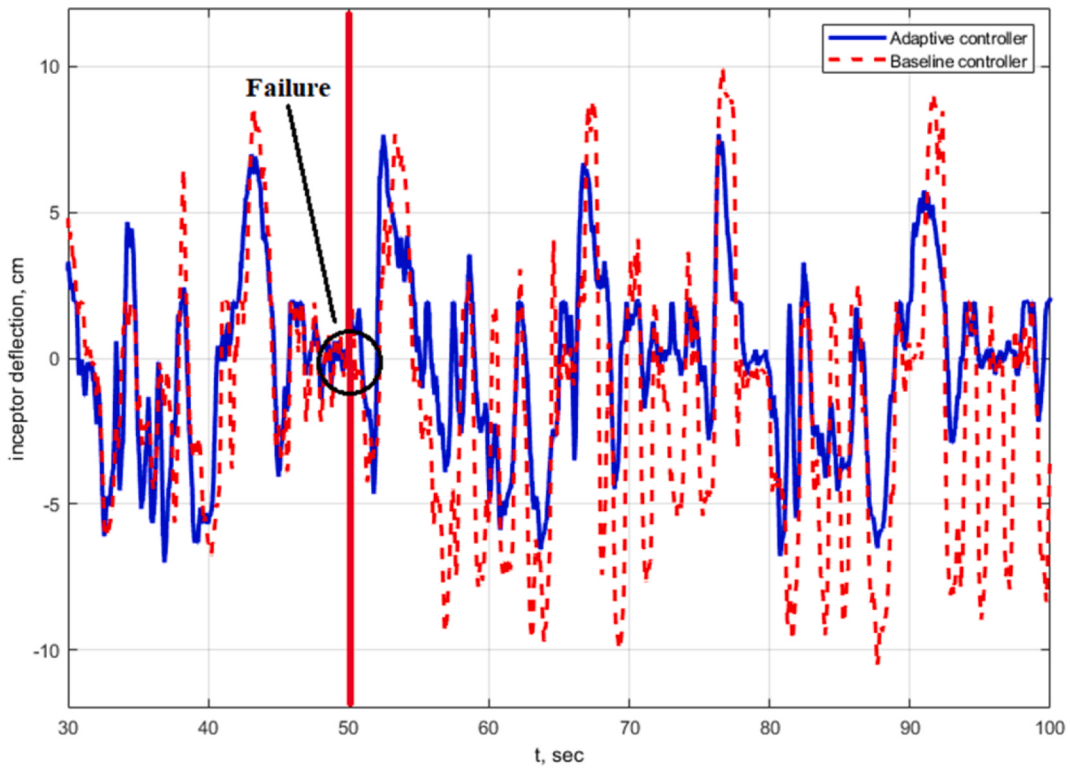
Fig. 13. Inceptor deflection in the case of a baseline and adaptive controller.

Table 2
Variances of error, σ_e^2, cm^2

	Baseline	Adaptive
Before failure	0.2405	0.2190
Sudden "α failure"	0.2926	0.2342
Sudden "elevator failure"	0.3603	0.2615

2) experiments on the assessment of adaptive augmentation (an NDI controller with online identification).

The first set of experiments was designed as a single-loop compensatory task (see Fig. 4 where Y_P is the pilot and Y_C is the controlled element dynamics.).

The pilot had to complete a pitch tracking task with a polyharmonic input signal represented by Equation (18), which appeared to them as a random signal.
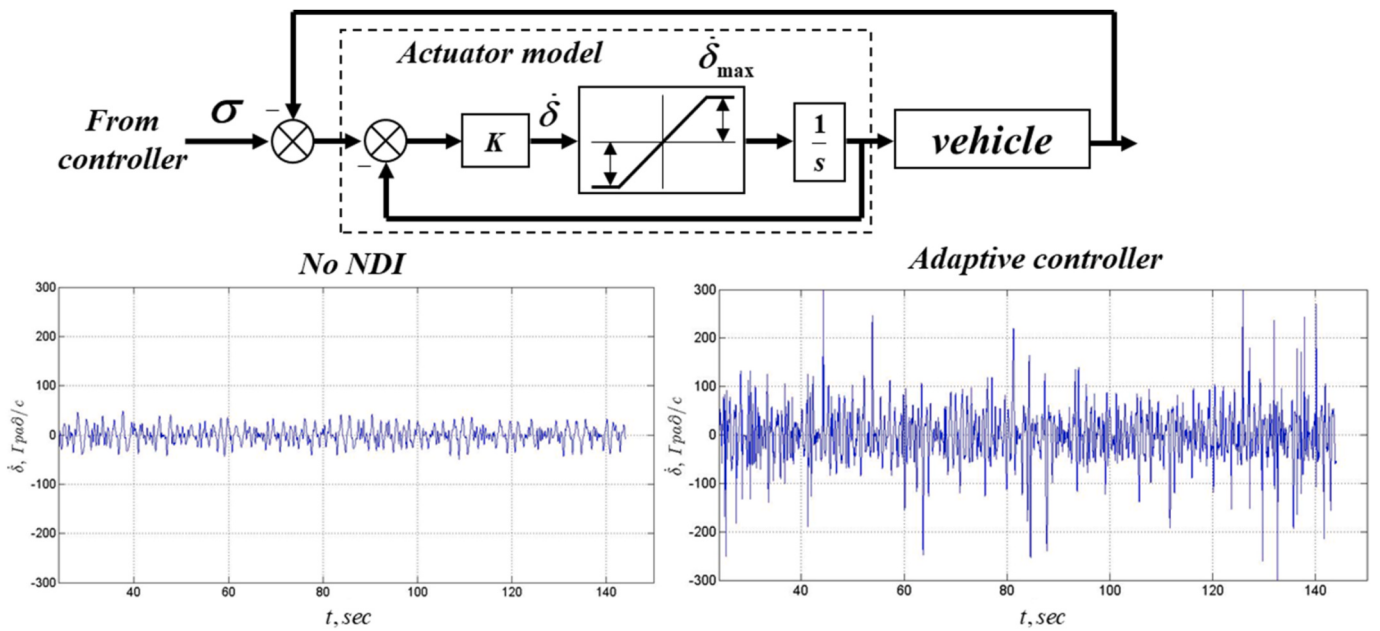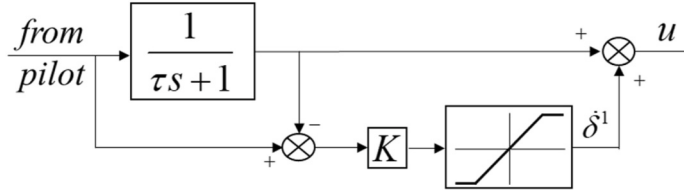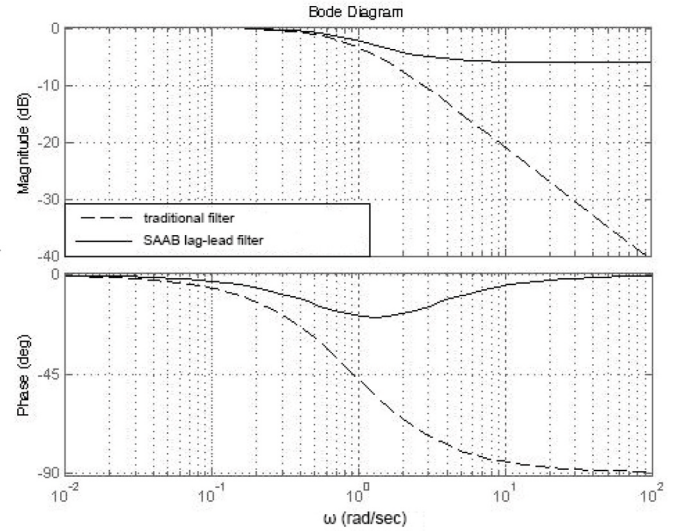
Fig. 14. Actuator-vehicle system and rates of control surfaces deflection.

Fig. 15. SAAB nonlinear lead-lag filter (a) and its frequency response (b).
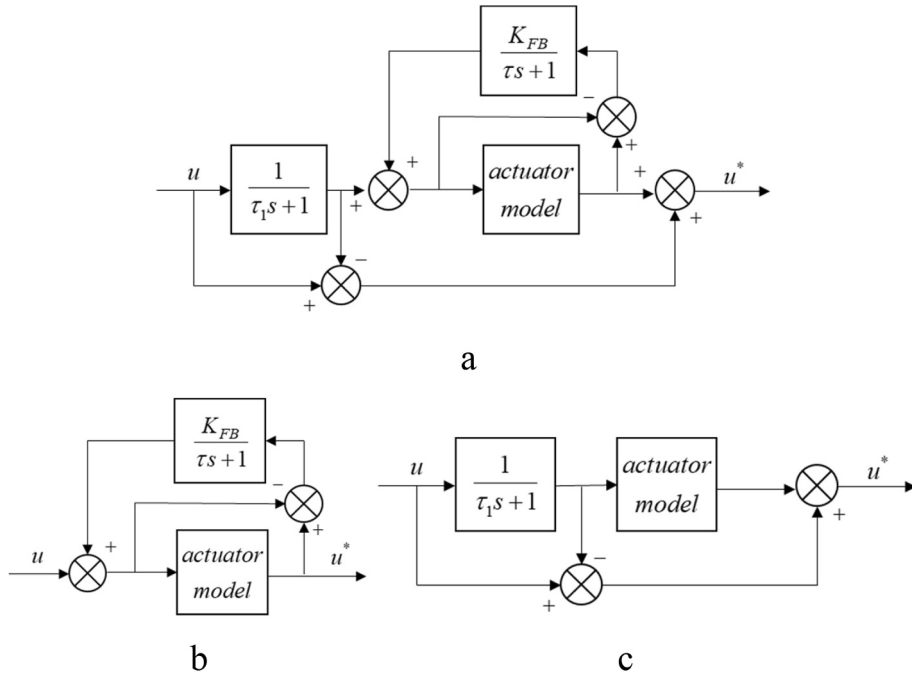
Fig. 16. Rate limiter with feedback and bypass prefilters and its subsystems.

$$i(t) = \sum_{k=1}^{15} A_k \cos \omega_k t \qquad (18)$$

The amplitudes A_k and orthogonal frequencies $\omega_k = K 2\pi/T$, where T is the duration of the experiment ($T = 144$ s), were selected according to the requirement of correspondence between the power distributions of the polyharmonic signal and a random signal characterized by the spectral density $\frac{K}{(\omega^2 + 0.5^2)^2}$ with the variance $\sigma_i^2 = 4 \deg^2$. The 15 frequencies ω_k covered the range from 0.26 rad/s to 15.71 rad/s. The selected frequencies and amplitudes were used extensively in the research performed at Moscow Aviation Institute [12,46]. Analysis demonstrated that this set of frequencies did not allow the pilot to predict the input signal. The Fourier coefficient technique described in

Ref. [46] was used to calculate the main pilot-vehicle system characteristics (the frequency response and the variance of error).

Three operators (one test pilot and two engineers) participated in the experiments. All of the experiments in this set were performed using MAI's ground-based workstation (see Fig. 5) equipped with a sidestick and a display demonstrating the error signal and two metrics: the desired d_{des} and adequate d_{ad} performance (1.75 cm and 2.54 cm, respectively [47]).

The effectiveness of a controller based on dynamic inversion (basic controller) was assessed for the Space Shuttle vehicle dynamics with all its additional filters and conditions of flight as considered in Ref. [19], as well as the SST dynamics. For each vehicle, two sets of experiments were conducted with and without a dynamic inversion controller. After the experiments, the variance of error σ_e^2 and its components determined by
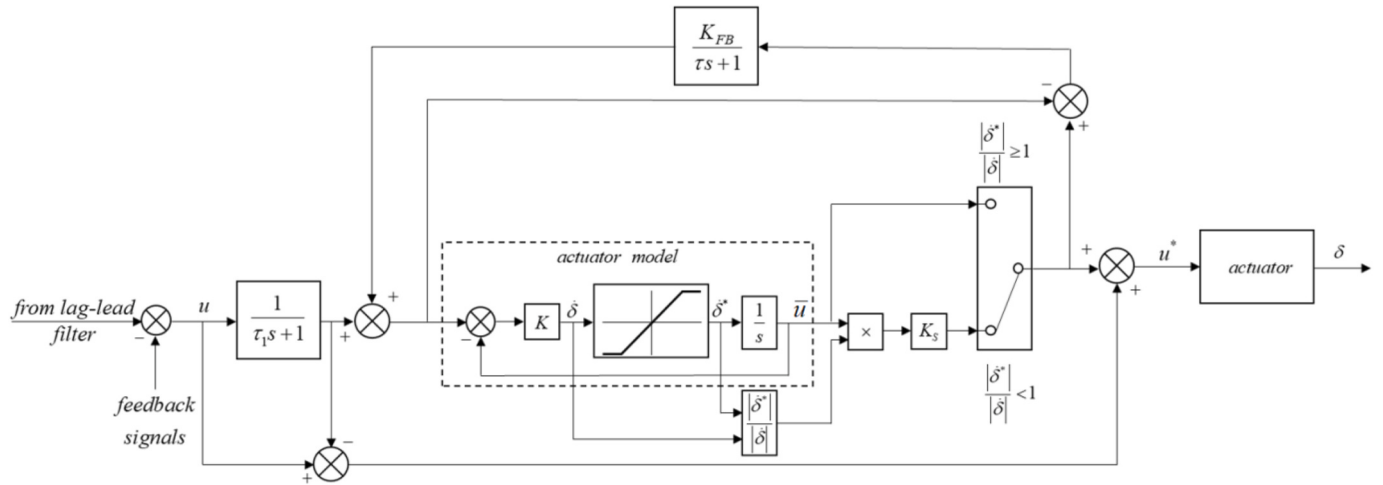
**Fig. 17.** Modified nonlinear rate limiter with feedback and bypass.
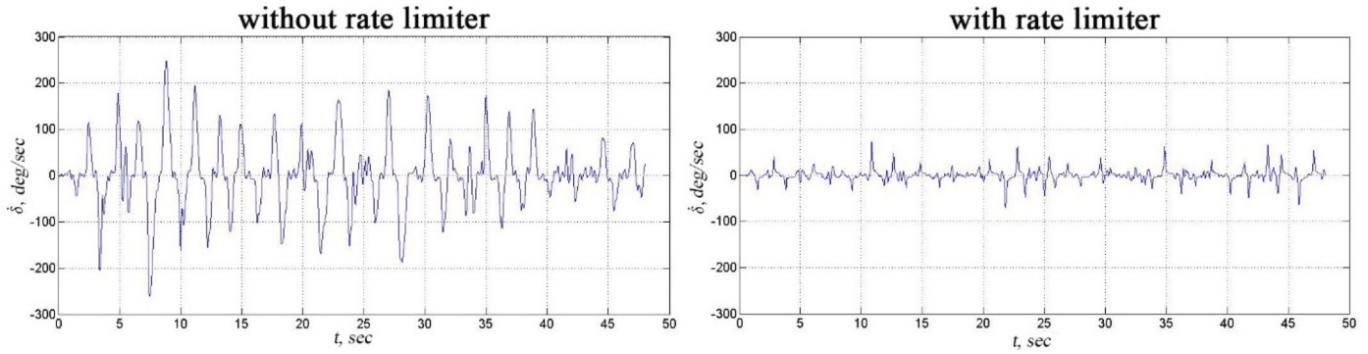
Fig. 18. Required rates of the actuator.

the input (σ_{ei}^2) and the remnant (σ_{en}^2) signals, frequency response characteristics (pilot $Y_P(j\omega)$, open-loop, and closed-loop system), and spectral density of the pilot remnant $S_{n_e n_e}$ were calculated using the Fourier coefficient technique.

The second set of experiments was dedicated to studying the effectiveness of an adaptive controller in nonstationary conditions. Two types of nonstationary conditions were studied:

1. Slow-changing vehicle dynamics during acceleration in level flight;
2. Sharp-changing vehicle dynamics due to a sensor failure which disabled angle of attack feedback ("α failure") and a decrease in elevator effectiveness ("elevator failure"). Angle of attack feedback is used in order to provide conventional short-period response.

Table 3
Variance of error.

| Controlled element dynamics	SST		Space Shuttle	
$\dot{\delta}_{max}$ Variant	30 *deg/sec*	15 *deg/sec*	30 *deg/sec*	15 *deg/sec*
Without limiter	0.709 *cm²*	0.959 *cm²*	0.399 *cm²*	1.293 *cm²*
SAAB rate limiter	0.357 *cm²*	0.800 *cm²*	0.543 *cm²*	1.780 *cm²*
Modified rate limiter	0.277 *cm²*	0.596 *cm²*	0.366 *cm²*	0.634 *cm²*

a

b
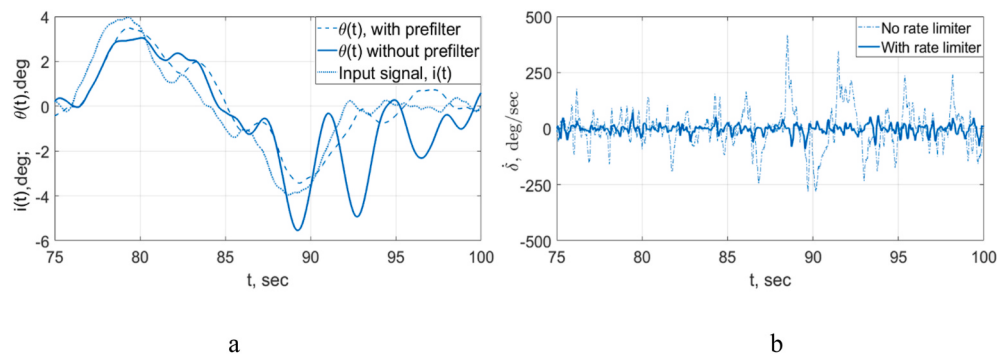
Fig. 19. PIOs in the Space Shuttle experiment (a); the required rates of the actuator (b).

A study of the first type of nonstationary conditions was performed under atmospheric turbulence simulated according to the scheme shown in Fig. 6. The set of frequencies in the disturbance signal $w_g(t)$ corresponded to the set used in the first group of experiments and the variance of this signal, $\sigma_w^2 = 4 \ m^2/sec^2$. Two types of SST controllers were considered: a baseline controller (NDI with fixed coefficients) and an NDI controller with adaptive augmentation (adaptive controller). The experiments started with preliminary trimmed flight at $V = 300$ km/h and $h = 1000 \ m$. After several seconds, the pilot increased the thrust to begin acceleration and tried to keep a constant altitude ($h = 1000 \ m, \dot{h} = 0$). In the frame of the second type of nonstationary conditions, two piloting tasks were performed: acceleration in level flight and an pitch tracking task. The acceleration in level flight was performed under the same conditions as considered above. The single difference was that at the moment $t = 15$ s, an "α failure" was introduced. The addition of turbulence did not allow the pilot to identify the moment of failure (see Fig. 7).

The pitch tracking task was performed with a constant speed $V = 267$ km/h, $h = 500 \ m$, and the same input signal as was used in the first groups of experiments. The following cases were studied:

(1) "Without failure": Experiments were performed with α feedback functioning for the whole duration of the experiment;
(2) "Sudden failure": Experiments started at normal conditions, and an "α failure" and "elevator failure" were introduced after 50 s.

Two types of SST controllers were studied in this piloting tasks: a baseline NDI controller ("baseline") and an NDI controller with adaptive augmentation ("adaptive").

The second set of experiments was performed using MAI's ground-based simulator (see Fig. 6). It has a computer-generated visual system with a frame rate of 60 Hz and the screen provides a 180 *deg* horizontal and 50 *deg* vertical angles of view. The cockpit is equipped with a primary display and other indicators, a central stick, pedals, and a throttle lever.

Each combination of vehicle and controller types in each set of experiments were given at least 5 trials by each operator and then the results of measuring the variance of error were averaged. The frequency response characteristics obtained in the first set of experiments were averaged as well. The frequency response characteristics obtained in the second set of experiments were averaged for one of the operators. Similar characteristics were obtained for the other operators as well. All of the experiments were performed by 3 operators (one test pilot and two engineers with years of experience in ground-based simulations for flying qualities evaluation).

3.2.2. Baseline controller

The results shown in Fig. 8 demonstrate that the dynamic inversion controller changes the controlled element dynamics considerably and such that the pilot does not need to introduce significant lead compensation. Additionally, the crossover frequency increased from 2 up to 2.6 rad/s, the bandwidth of the closed-loop system increased from 2.6 up to 3.4 rad/s, and the variance of error decreased by a factor of 2.

The bandwidth of vehicle dynamics $\omega_{BW\theta}$ increased from 1.3 rad/s to 3.1 rad/s, and the equivalent time delay $\tau_{e\theta}$ in the pitch tracking task decreased from 0.2 s to 0.1 s. Using such flying qualities criteria as criterion "$\omega_{BW\theta}$ and $\tau_{e\theta}$" [47], allowing to predict the level of pilot rating PR, or the criterion for calculating a pilot rating [12]:

$$PR = 1 + 5.36 \ln \sigma_e/\sigma_{e \ opt} \qquad (19)$$

where σ_e and $\sigma_{e \ opt}$ are mean squares obtained for the considered controlled element dynamics or optimal dynamics [46], it is possible to estimate the pilot ratings for the basic Space Shuttle flight control system (PR_b) and its proposed adaptive version (PR_{ad}) (see Table 1).

In criterion (19) the PR_b and PR_{ad} were calculated with taking into account that $\sigma_{e \ opt}$ for the considered spectrum of input is equal to 0.25 cm and the standard deviation of error σ_e corresponded to the results of the experiments (see Fig. 8).

According to Refs. [12,47], the rating PR determines the probability of an accident due to pilot error when performing manual control in the following way:

$$P(PR) = C_9^{PR-1} p^{PR-1} (1-p)^{10-PR} \qquad (20)$$

$$p = \frac{\overline{PR} - 1}{9}; \ C_9^{PR-1} = \frac{9!}{(PR-1)!(10-PR)!} \qquad (21)$$

$\overline{PR}$ is the mean of pilot rating PR.

Taking into account the data given in Table 1, we can conclude that the using the adaptive controller allows to decrease the probability of accidents from 10^{-2} to $5 \cdot 10^{-4} - 10^{-5}$.

3.2.3. Adaptive augmentation

The experiments with acceleration in level flight with slow-changing vehicle dynamics demonstrated that in case of an adaptive controller, the variance of error σ_e^2 is on average 2.7 times less in comparison with the case when a baseline controller (NDI with fixed coefficients) is used (see Fig. 9).

The same piloting task performed in conditions of an "α failure" was accompanied by the oscillations of $\dot{h}(t)$ and angle of attack $\alpha (t)$ (see Fig. 10) in experiments where the controller was based on feedbacks only (no NDI). In the case of an adaptive controller, such oscillations are not taken place. As can be seen in Fig. 11, in the case where there is a sudden "elevator failure" (a decrease in the elements of matrix B by 50%), adaptive augmentation takes roughly 3 s to converge to the new values of the matrix.

This procedure allows to maintain the pilot amplitude response (see Fig. 12). The averaged pilot amplitude responses $|Y_P(j\omega)|$, obtained by one of the operators in the case of an adaptive controller stayed practically the same as in the case where experiments were performed without an "elevator failure". The time response of inceptor deflection $c (t)$ shown in Fig. 13 confirms that an elevator failure occurring at the 50th second practically does not influence the amplitudes of $c(t)$ in the case of an adaptive controller and increases considerably after the failure in experiments with a baseline controller. The use of an adaptive controller led to a decrease in the variance of error by up to 40% in comparison with a baseline controller (see Table 2).

In the case of a sudden "α failure", the adaptive controller provided a decrease in error by 2.2 times in comparison with the baseline version. Sudden "α and elevator failures" cause a deterioration in piloting accuracy for both variants of the controller. However, such deterioration is considerably more pronounced in the case of a baseline controller: 3 and 3.3 times greater in the case of "elevator and α failures", respectively, in comparison with an adaptive controller.

4. Alternative versions of nonlinear prefilters

4.1. Algorithms of nonlinear prefilters

The implementation of the dynamic inversion controller is accompanied by high values of the required rates of control surfaces deflection $\dot{\delta}(t)$ (see Fig. 14) [48].

To counteract this effect and improve flight safety, it is proposed to install a modified version of the SAAB rate limiter [43] in the flight control system. It consists of two elements: a nonlinear lead-lag filter and a feedback-with-bypass (FWB) rate limiter. The former, shown in Fig. 15a, limits the pilot control signal. In comparison with traditional prefilters, it decreases delay in phase response (see Fig. 15b).

The FWB (see Fig. 16a) rate limiter limits the actuator input signal. It

consists of two subsystems. One of them is a prefilter with feedback (see Fig. 16b) and the other is a prefilter with lead compensation (see Fig. 16c). Both of them contain a simplified nonlinear model of the actuator. It is possible to shown that for $T_1 = 0.05$ s, $K_{FB} = 8$, $T = 1$ and $\tau = 0.1$ s. The first subsystem provides the phase delay lead in the frequency range of 0.1–10 rad/s and the second provides the phase lead in the frequency range higher than 10 rad/s.

The modified version of the SAAB rate limiter included the MAI rate limiter [49]. Its principle is based on a comparison of the signals $\dot{\delta}$ and $\dot{\delta}^*$, which are the input and output signals of the rate limiting element in the actuator model. If the signal $\dot{\delta}$ is less than the rate limit $\dot{\delta}^*$, then the prefilter output is not corrected. Otherwise, the input signal "$\overline{u}$" is multiplied on the ratio $\frac{|\dot{\delta}^*|}{|\dot{\delta}|}$ and the gain coefficient $K_S = 0.9$–1.1. In that case, the actuator signal u^* decreases. This allows to reduce the PIO tendency. The combination of the MAI and FWB rate limiters is shown in Fig. 17.

4.2. Experimental assessment of effectiveness of the proposed rate limiter

The experiments on the effectiveness of the proposed rate limiter were performed using the workstation by the same group of operators participating in the experiments on the assessment of the adaptive controller. The procedure for the experiments, including the averaging of results and input signal, were also the same.

The use of the modified version of SAAB rate limiter demonstrated its high effectiveness especially in case of small values of $\dot{\delta}_{\max}$ for the second-generation SST and the Space Shuttle. In the experiments, the mathematical models of the flight control systems of both vehicles included an adaptive controller based on the inverse dynamics principle. The results of the experiments in which operators performed a pitch tracking task with SST at MAI workstation are shown in Fig. 18 and Table 3. It can be seen that the proposed prefilter allows to considerably decrease the rates of $\dot{\delta}$.

The same results were also obtained for the Space Shuttle in the same piloting task (see Fig. 19a). The considerable $\dot{\delta}(t)$, arising periodically, causes the appearance of oscillations (see Fig. 19b). The installation of the proposed limiter suppresses these effects.

In addition to the suppression of PIOs, the rate limiter provides a decreasing in the variance of error for the SST, as well as for the Space Shuttle.

In the case of the Space Shuttle, whose dynamics are characterized by considerable time delay unlike the SST dynamics, the use of the SAAB rate limiter allowed to decrease the required rates $\dot{\delta}$ in comparison with experiments performed without rates limits. In spite of this, the task performance (σ_e^2) was 1.36–1.37 times higher for both maximum rate limits – 15 and 30 *deg/sec* (see Table 3). The experiments performed with the modified rate limiter demonstrated a considerable improvement in task performances for the SST, as well as the Space Shuttle. For the Space Shuttle, the greatest effect in decreasing error is noticed at the smallest rate limiting $\dot{\delta}_{\max} = 15$ deg/sec, which is close to its real rate limiting. For both vehicles, no unstable processes in manual control were registered when the proposed rate limiter was used.

5. Conclusion

This paper presents an adaptive controller based on the principle of dynamic inversion and simultaneous online identification of vehicle dynamics using a least square approach. The proposed online identification approach allows to obtain piecewise linear systems corresponding to the nonlinear vehicle dynamics with high accuracy.

The developed adaptive controller transforms the vehicle dynamics considerably, allows to decrease the variance of error by a factor of 2, and improves the pilot-vehicle system characteristics and flight safety. In particular, it is shown that the probability of an accident due to pilot

error in a reentry vehicle decreases from 10^{-2} (basic flight control system) to $5 \cdot 10^{-4} \div 10^{-5}$ (modified flight control system).

Experimental studies also demonstrated that, on both vehicles considered, the effects of system failures are completely suppressed when using the adaptive controller, and PIOs are eliminated.

In addition to the adaptive controller, the paper presents a rate limiter that allows to considerably decrease the high actuator rates required by the adaptive controller. In the case of a reentry vehicle, its use provides a decrease in the variance of error by a factor of 2. It also eliminates oscillations in the closed-loop system and, as a consequence, improves flight safety.

Declaration of competing interest

The authors declare that they have no known competing financial interests or personal relationships that could have appeared to influence the work reported in this paper.

Acknowledgments

References

[1] E.P. Buslov, I.S. Komarov, V.V. Selivanov, V.A. Titov, N.A. Tovarnova, V. A. Feldstein, Protection of inflatable modules of orbital stations against impacts of particles of space debris, Acta Astronaut. 163 (2019) 54–61.

[2] V.V. Adushkin, O.Y. Aksenov, S.S. Veniaminov, S.I. Kozlov, V.V. Tyurenkova, The small orbital debris population and its impact on space activities and ecological safety, Acta Astronaut. 176 (2020) 591–597.

[3] A.M. Tereza, S.P. Medvedev, V.N. Smirnov, Experimental study and numerical simulation of chemiluminescence emission during the self-ignition of hydrocarbon fuels, Acta Astronaut. 163 (2019) 18–24.

[4] G. Jomaas, J.L. Torero, C. Eigenbrod, J. Niehaus, S.L. Olson, P.V. Ferkul, G. Legros, A.C. Fernandez-Pello, A.J. Cowlard, S. Rouvreau, N. Smirnov, O. Fujita, J.S. T'ien, G.A. Ruff, D.L. Urband, Fire safety in space–beyond flammability testing of small samples, Acta Astronaut. 109 (2015) 208–216.

[5] A.S. Melikhov, I.A. Bolodyan, L.T. Tanklevskiy, Fire safety provision in inhabited pressurized compartments of spacecraft during a flight in simulated gravity, Acta Astronaut. 176 (2020) 725–732.

[6] M.Y. Marov, Radiation and space flights safety: an insight, Acta Astronaut. 176 (2020) 580–590.

[7] Z. Wang, Z. Wu, Y. Du, Robust adaptive backstepping control for reentry reusable launch vehicles, Acta Astronaut. 126 (2016) 258–264.

[8] H. Yang, X. You, C. Hua, Attitude tracking control for spacecraft formation with time-varying delays and switching topology, Acta Astronaut. 126 (2016) 98–108.

[9] D.H. Klyde, D.G. Mitchell, Investigating the role of rate limiting in pilot-induced oscillations, J. Guid. Control Dynam. 27 (No. 5) (2004) 804–813.

[10] D.L. Hirsch, R.L. McCormick, Experimental investigation of pilot dynamics in a pilot-induced oscillation situation, J. Aircraft 3 (No. 6) (1966) 567–573.

[11] A. Steer, Flight Control for Advanced Supersonic Transport Aircraft Handling Quality Design, Canfields University Ph.D. thesis, 2000, pp. 1–222.

[12] A.V. Efremov, Pilot-Aircraft System. Regularities and Mathematical Models of Pilot Behavior, MAI, 2017, pp. 1–193.

[13] A.V. Efremov, M.S. Tyaglik, I.Kh Irgaleev, E.V. Efremov, T.V. Voronka, Methodology for Assessing the Risks of the Human Factor Due to Pilot Errors in the Process of Piloting an Aircraft, Russian Aeronautics, 2020, pp. 241–248.

[14] J.W. Smith, Analysis of a Longitudinal Pilot-Induced Oscillation Experienced on the Approach and Landing Test of the Space Shuttle, 1981. NASA-TM-81366.

[15] D.T. McRuer, Pilot-Induced Oscillations and Human Dynamic Behavior, 1995. H-2042, NASA CR-4683.

[16] D.T. McRuer, Aviation Safety and Pilot Control: on the Effects of Aircraft Pilot Coupling on Flight Safety, National Academy Press, 1997, pp. 1–189.

[17] G.S. Bushgens, Aerodynamics, Stability and Controllability of Supersonic Aircraft, Zhukovsky Central Aerodynamic Institute, Moscow, 1998, pp. 1–816. Nauka-Fizmatlit.

[18] A.V. Efremov, A.V. Ogloblin, Development and application of the methods for pilot-aircraft system research to the manual control tasks of modern vehicles, AGARD Conference Proceedings No 556 (1995) 15-1–15-12.

[19] T.T. Myers, D.E. Johnston, D.T. McRuer, *Space Shuttle Flying Qualities And Criteria Assessment*, NASA Contractor, 1987, pp. 1–203. Report 4049, Ames Research Center Dryden Flight Research Facility under Contract NAS2-11900.

[20] B.G. Powers, An adaptive stick-gain to reduce pilot-induced oscillation tendencies, J. Guid. Control Dynam. 5 (No. 2) (1982) 138–142.

[21] C. Miller, Nonlinear Dynamic Inversion Baseline Control Law: Architecture and Performance Predictions, AIAA Guidance, Navigation, and Control Conference, 2011, pp. 6467–6492.

[22] R.R. Da Costa, Q.P. Chu, J.A. Mulder, Reentry flight controller design using nonlinear dynamic inversion, J. Spacecraft Rockets 40 (No. 1) (2003) 64–71.

[23] G. Wu, X. Meng, F. Wang, Improved nonlinear dynamic inversion control for a flexible air-breathing hypersonic vehicle, Aero. Sci. Technol. 78 (2018) 734–743.

[24] J. Reiner, G.J. Balas, W.L. Garrard, Flight control design using robust dynamic inversion and time-scale separation, Automatica 32 (No. 11) (1996) 1493–1504.

[25] H. Lee, S. Reiman, C. Dillon, H. Youssef, Robust Nonlinear Dynamic Inversion Control for a Hypersonic Cruise Vehicle, AIAA Guidance, Navigation, and Control Conference and Exhibit, 2007, p. 6685.

[26] A. Hodel, M. Whorton, J. Zhu, Stability Metrics for Simulation and Flight-Software Assessment and Monitoring of Adaptive Control Assist Compensators, AIAA Guidance, Navigation, and Control Conference and Exhibit, 2008, p. 7005.

[27] P. Smith, A Simplified Approach to Nonlinear Dynamic Inversion Based Flight Control, 23rd Atmospheric Flight Mechanics Conference, 2008, p. 4461.

[28] B.J. Bacon, A.J. Ostroff, S.M. Joshi, Reconfigurable NDI controller using inertial sensor failure detection & isolation, IEEE Trans. Aero. Electron. Syst. 37 (No. 4) (2001) 1373–1383.

[29] P. Lu, E.J. Van Kampen, C. de Visser, Q. Chu, Aircraft fault-tolerant trajectory control using incremental nonlinear dynamic inversion, Control Eng. Pract. 57 (2016) 126–141.

[30] P. Simplício, M.D. Pavel, E. Van Kampen, Q.P. Chu, An acceleration measurements-based approach for helicopter nonlinear flight control using incremental nonlinear dynamic inversion, Control Eng. Pract. 21 (No. 8) (2013) 1065–1077.

[31] E.J. Smeur, G.C. de Croon, Q. Chu, Gust Disturbance Alleviation with Incremental Nonlinear Dynamic Inversion, IEEE/RSJ International Conference on Intelligent Robots and Systems (IROS), 2016, pp. 5626–5631, 2016.

[32] I. Matamoros, C.C. de Visser, Incremental Nonlinear Control Allocation for a Tailless Aircraft with Innovative Control Effectors, AIAA Guidance, Navigation, and Control Conference, 2018, p. 1116, 2018.

[33] W. Van Ekeren, G. Looye, R. Kuchar, Q. Chu, E.J. Van Kampen, Design, in: Implementation and Flight-Test of Incremental Backstepping Flight Control Laws, AIAA Guidance, Navigation, and Control Conference, 2018, pp. 1–21.

[34] Y. Huang, Y. Zhang, D.M. Pool, O. Stroosma, Q. Chu, Time-delay margin and robustness of incremental nonlinear dynamic inversion control, J. Guid. Control Dynam. 45 (No. 2) (2022) 394–404.

[35] W.J. Rugh, J.S. Shamma, Research on gain scheduling, Automatica 36 (No. 10) (2000) 1401–1425.

[36] D.J. Leith, W.E. Leithead, Survey of gain-scheduling analysis and design, Int. J. Control 73 (No. 11) (2000) 1001–1025.

[37] J.S. Shamma, M. Athans, Gain scheduling: potential hazards and possible remedies, IEEE Control Syst. Mag. 12 (No. 3) (1992) 101–107.

[38] A. Packard, Gain scheduling via linear fractional transformations, Syst. Control Lett. 22 (No. 2) (1994) 79–92.

[39] R.A. Nichols, R.T. Reichert, W.J. Rugh, Gain scheduling for H-infinity controllers: a flight control example, IEEE Trans. Control Syst. Technol. 1 (No. 2) (1993) 69–79.

[40] R.G. Berstecher, R. Palm, H.D. Unbehauen, An adaptive fuzzy sliding-mode controller, IEEE Trans. Ind. Electron. 48 (No. 1) (2001) 18–31.

[41] W. Wang, J. Yi, D. Zhao, D. Liu, Design of a stable sliding-mode controller for a class of second-order underactuated systems, IEE Proc. Control Theor. Appl. 151 (No. 6) (2004) 683–690.

[42] Y.P. Chen, S.C. Lo, Sliding-mode controller design for spacecraft attitude tracking maneuvers, IEEE Trans. Aero. Electron. Syst. 29 (No. 4) (1993) 1328–1333.

[43] L. Rundqwist, Rate limiters with phase compensation, Proceedings of 20th Congress of ICAS (1996) 2634–2642.

[44] B. Charlet, J. Lévine, R. Marino, On dynamic feedback linearization, Syst. Control Lett. 13 (No. 2) (1989) 143–151.

[45] T. Takagi, M. Sugeno, Fuzzy identification of systems and its applications to modeling and control, IEEE Transactions on Systems, Man, and Cybernetics 15 (No. 1) (1985) 116–132.

[46] A.V. Efremov, V.V. Rodchenko, S. Boris, Investigation of pilot induced oscillation tendency and prediction criteria development, in: Flight Dynamics Directorate, Wright Laboratory, 1996, pp. 1–138. WL-TR-96-3109.

[47] A.V. Efremov, E.V. Efremov, M.S. Tiaglik, Advancements in predictions of flying qualities, pilot-induced oscillation tendencies, and flight safety, J. Guid. Control Dynam. 43 (No. 1) (2020) 4–14.

[48] A.V. Efremov, Z. Mbikayi, E.V. Efremov, Comparative study of different algorithms for a flight control system design and the potentiality of their integration with a sidestick, Aerospace 8 (No. 11) (2021) 1–17.

[49] A.V. Efremov, A.I. Shcherbakov, F.A. Korzun, V.A. Prodanik, Prospective means of suppressing pilot-induced oscillations, Aerospace MAI Journal 29 (2022) 1–12.